OPTIMIZATION OF SOLAR CELL SHIELDING FOR GEOSTATIONARY MISSIONS

M. W. Walkden

Royal Aircraft Establishment
Farnborough, England

August 1973

TR 73105

AUGUST 1973

ROYAL AIRCRAFT ESTABLISHMENT

TECHNICAL REPORT 73105

OPTIMISATION OF SOLAR CELL SHIELDING FOR GEOSTATIONARY MISSIONS

by

M. W. Walkden

PROCUREMENT EXECUTIVE, MINISTRY OF DEFENCE
FARNBOROUGH, HANTS

UDC 629.19.066.5 : 629.195.521.26 : 629.199.81

ROYAL AIRCRAFT ESTABLISHMENT

Technical Report 73105

Received for printing 15 June 1973

OPTIMISATION OF SOLAR CELL SHIELDING FOR GEOSTATIONARY MISSIONS

by

M. W. Walkden

SUMMARY

Equivalent 1MeV electron fluences, end of life output powers and power to weight ratios are estimated for solar cells in a five year geostationary mission beginning in 1975. The study covers cell thicknesses from 125 μm to 300 μm, coverslip thicknesses from 25 μm to 300 μm, and rear shielding typical of rigid and lightweight flexible arrays.

It is concluded that the thinnest cells and shielding give the best power to weight ratio, although the choice for a particular spacecraft will be influenced by considerations of availability, cost, fragility and array area.

Departmental Reference: Space 434

CONTENTS

1 INTRODUCTION

Geostationary communication satellites of the future will require more power. For this reason, there is likely to be a change from the present spinning satellites with their body mounted solar cells, to 3 axis stabilised spacecraft with large sun orientated arrays.

Such arrays, particularly if efforts are made to reduce weight by using thinner cells, coverslips and substrates, are more susceptible to radiation damage than the present configuration, and the array designer needs data to enable him to choose the optimum combination for a particular mission, and to estimate the probable end-of-life output power of his selected design.

In the present report, end-of-life maximum powers and power to weight ratios are derived for three thicknesses of 20mm × 20mm solar cell with six thicknesses of coverslip and three rear shield variants, after a five year geostationary mission beginning in 1975. The variants selected are either currently available or expected to be in the near future.

This approach was considered to be less time consuming and more relevant to present needs than a complete analytical study.

Factors which determine the damage experienced by the solar cell array are the radiation environment, the time spent in that environment, and the protection from protons and electrons afforded by the solar cell coverslip at the front, and the cell substrate, etc. at the rear.

This Report uses published data of the annual solar flare proton and trapped electron fluxes[1] which spacecraft would experience at geostationary altitude in the period 1975-77. Energy dependent damage factors for various front cover/cell/rear shield combinations, which relate protons and electrons of various energies to a monoenergetic electron flux (1 MeV) are multiplied by the proton and electron populations over the energy range and summed to give an equivalent 1MeV electron fluence. This fluence is extrapolated for a five year mission starting in 1975 by taking account of the variation in solar activity during this period[2].

The solar cell maximum power outputs at the end of the five year mission are then derived from recent RAE experimental 1MeV electron degradation data and the power to weight ratios of the various combinations calculated.

2 COVERSLIP/CELL/REAR SHIELD VARIANTS

The variants selected for study are listed in Table 1.

Three thicknesses of cell are usually obtainable from the cell manufacturer; 125 μm, 200 μm and 300 μm, the thinner the cell, higher the cost. Discrete individually mounted coverslips are obtainable in 100, 150 and 300μm thicknesses. Recent reported advances[3] in the deposition of integral cover glasses open the way for the use of thinner covers, and integral covers down to 25 μm were considered.

Two types of rear shield were taken into account - the folded flexible and the fold-up rigid. The flexible type was based on the design of the RAE lightweight flexible array[4]. This is 8 μm of cell positive contact, plus 50 μm of Silastoseal B adhesive, covering the whole cell and used for a highly emissive thermal finish, plus 50μm Kapton polyimide substrate covering half the cell area, plus 25 μm of molybdenum for the four quarters of the cell interconnection rings, all scaled in the ratio of their respective areas. This shield was estimated to have a stopping power of 17 mg cm^{-2}. In order to establish how critical the substrate is to the cell shielding another case with the cell contact and Silastoseal B only was included.

For the rigid fold-up panel, two cases were considered, the thinnest practicable -100 μm of aluminium (34 mg cm^{-2}) and the thickest possible - infinite rear shielding.

3 ORBITAL ENVIRONMENT

Charged particle radiations at geosynchronous altitude include trapped protons and electrons, alpha particles, solar flare protons and galactic cosmic rays.

Of these, by far the most damaging to solar arrays are solar flare protons and trapped electrons. Providing the cell is completely covered, low energy trapped protons are insignificant in their effect. Source data for the latter two radiations applicable for the years 1975-77 were taken from Ref.1, and are shown in Figs.1 and 2 respectively. The data were the source of the differential fluxes used to compute the equivalent 1MeV electron flux described in section 4.

The peak of the 21st sun cycle is expected to occur about 1980-82, so that if a five year mission commencing in 1975 is considered, some allowance must be made for the increased solar activity and consequential solar flare proton fluxes which will occur in the years preceding the peak. Annual proton fluxes

in 1980-82 are expected to be an order of magnitude greater than the average for 1974-77[2], and those in the period 1978-79 about five times greater. If these values are smoothed for the five years 1975-80, it is evident that the average annual solar flare proton flux in 1975-77 should be multiplied by a factor of 10 for the five year period. This was done, but it should be pointed out that because of the uncertainty of solar flares, the predicted proton fluences may be in error by a factor of up to two.

The trapped electron fluxes do not vary significantly from year to year and therefore no similar correction is necessary in this case.

4 SOLAR CELL DAMAGE FACTORS

4.1 Definition

Solar cell damage factors used to convert the proton and electron populations to equivalent 1MeV electron fluxes are defined as:-
The number of protons or electrons of a particular energy required to produce 25% degradation in maximum power, divided by the number of 1MeV electrons to produce the same maximum power degradation.

4.2 Front incidence protons

Damage factors for normal incidence protons of energies from 2 to 155 MeV were derived experimentally[5] in 1971. Fig.3 shows the values for 2 to 100 MeV for uncovered cells. The thinnest cover slides used in this study were 150 μm and 300 μm. In order to obtain damage factors for cells with thinner covers, the mass range of protons in SiO_2 (Fig.4) was used to determine Fig.5, which shows the exit *versus* incident energies for the cover thicknesses considered. These data were then applied to Fig.3. Damage factors obtained in this way for covers of 25, 50, 75 and 100 μm are shown in Fig.6. Also shown are the experimental curves for 150 and 300 μm, which were in good agreement with calculated values. These covers have identical damage factors for energies greater than 20 MeV, and the four thinner covers for energies in excess of 10 MeV. It was assumed that all cell thicknesses have the same front damage factors.

4.3 Rear incidence protons

No measured damage factors are known to exist for rear incidence protons; however an approximate solution is postulated below.

Referring to Fig.7, when a proton is absorbed in a solar cell, most of the damage which results is done in the region where the proton comes to rest. Thus, normal incidence protons of energy E_R produce a damage stratum at a depth R_1, which is a function of the incident energy and the rear shielding. Fig.8 illustrates this dependence. Subtraction of R_1 from the cell thickness, t, gives a second range, R_2, for which the energy E_F, of the equivalent front entry proton may be found from Fig.9. The damage factor K_F corresponding to energy E_F, as derived from Fig.3, may then be taken as the appropriate damage factor for rear incidence protons of energy E_R. Although the approximation breaks down for protons which come to rest near the front and rear surfaces, it is sufficient to give a general shape of the damage factor curve for the shields considered. Damage factors derived in this way for the three cell thicknesses and the three rear shields are shown in Figs.10, 11 and 12, where it may be seen that for the variants considered, the damage factors are identical for energies greater than 10 MeV.

4.4 Electrons

Electron damage factors for energies of 1, 1.8 and 4 MeV for 10 ohm cm silicon solar cells were derived experimentally in 1968[6]. As these were for uncovered cells, the effect of the front covers on the incident electron energy was calculated in similar fashion as for the protons. The mass range of electrons in SiO_2 is shown in Fig.13, and the consequent attenuation of energy for the front covers is shown in Fig.14. From these data the electron damage factors for cells fitted with the six coverslips have been calculated and are shown in Fig.15. As the damage mechanism for electron penetration is primarily a collision knock-on process, the damage is not in discrete strata as in the case of protons, but is assumed to be uniformly distributed throughout the thickness of the cell. Therefore electrons leaving the shield with a particular energy are assumed to have the same effect on the cell whether they are incident from the front or the rear. Fig.16 shows the incident *versus* exit energies for the three rear shields, and Fig.17, the consequent damage factors.

5 EQUIVALENT 1MeV ELECTRON FLUX

The differential flux in narrow energy bands was obtained from Figs.1 and 2. The widths of the bands in the case of protons was selected to be finest in the region where:-

(a) damage factors are greatest

(b) damage factors are changing most rapidly

(c) fluxes are highest.

The proton energy bandwidths used were:-

Range	Bandwidth
1-10 MeV	0.5 MeV
10-20 MeV	2.0 MeV
20-100 MeV	10 MeV

In the case of electrons 0.2MeV intervals were used over the whole range.

It was assumed half the differential flux in each energy band was incident normally on the front cover surface and the other half on the rear shield surface.

This simplification is discussed below. Referring to Fig.18, a proton of energy E enters a cover normally and after attenuation enters the cell with energy E_1, where it has a range R_1 in the cell, producing a damage factor K_1. Another proton of the same energy enters the cover at angle θ to the normal. The path through the cover is longer by $1/\cos\theta$ and the energy is attenuated to E_2. The range R_2 in the cell is therefore less, and the proton will be absorbed nearer the cell p/n junction and hence produce a higher damage factor, K_2. Another proton of the same energy entering the cover at angle ϕ has insufficient energy to traverse the effective thickness of the cover and thus produces no damage to the cell.

In short, for a particular energy and cover/cell combination, the proton damage factor increases initially as the angle of incidence is increased from normal but when a critical angle is reached it falls to zero. The effects of omnidirectional incidence are therefore to some extent self cancelling.

Because of this, and bearing in mind the uncertainties of solar flare prediction and the complexities of partial shielding of the array by the spacecraft body, it was decided that an attempt to modify the damage factors to take account of an omnidirectional flux would not be justified. Although some error is inherent in the simplified approach, it is likely to be an order of magnitude less than the estimates of the solar flare proton and electron fluxes.

The damage factors for the front and rear shield variants under consideration were obtained from the appropriate curves, (Fig.6, 10, 11, 12, 16 or 17), at the mid-energy point of the band. Each was then multiplied by half the differential flux in the band and the products summed. This was done at progressively higher energies until further increments produced no significant increase in the accumulated sum.

A breakdown of the proton and electron components of the equivalent 1MeV electron flux for front and rear incidence irradiations is shown in Tables 2 and 3 respectively. Table 4 shows the total equivalent 1MeV electron flux from both front and rear incidence. Also given is the flux through the front cover only, which may be used in calculations for body-mounted array where the rear shield is practically infinite. The data given in these tables are applicable only for the years 1975-77.

Table 5 shows the equivalent 1MeV electron flux for the five year period 1975-80. As stated in section 1, the equivalent 1MeV electron flux derived from the solar flare proton environment (Tables 2 and 3) was multiplied by 10 and that from the electron environment by a factor of 5. Again the effects of all front and rear covers and infinite shields are shown.

6 POWER-TO-WEIGHT RATIO

Performance data used in the computation of power-to-weight ratio were taken from RAE measurements on a small sample of Ferranti ZMS 051024 FW, (MS 36), solar cells. This recently introduced type measures 20 mm × 20 mm × 125 μm, is fabricated from 10ohm cm float zone silicon and has wrap around contacts (i.e. both negative and positive on the back). It has 24 off, 25μm wide fingers on the active surface, in place of the former 6 off, 100μm wide finger pattern (MS 23). Thus the same active area is maintained with reduced internal resistance. This, together with diffusion and anti-reflection coating improvements, has resulted in enhanced maximum power output. The voltage current characteristics at 25°C for both types of cell is shown in Fig.19, the maximum power *versus* 1MeV electron fluence is shown in Fig.20.

The maximum steady state temperature of cells in the RAE lightweight array has been estimated[7] as 62°C. The performance of the MS 36 at this temperature is included in Fig.20.

No comparable cell characteristics are at present available for 200μm and 300μm thick cells. However it is shown in section 5, that the equivalent

1MeV electron fluence for the five year mission is, in general, in excess of 10^{15} 1 MeV e cm^{-2}. After this fluence, both 200μm and 300μm cells will have degraded to give sensibly the same output as the 125μm cell[7]. The maximum power output curves for 200μm and 300μm cells have therefore been assumed to be identical to that for the 125μm cell.

The actual cells used for the performance measurements were weighed and their thickness measured to determine *pro rata* the weights of the other cell thicknesses. Weights of the coverslips were calculated assuming a density of 2.32 g cm^{-3}.

The specific mass of a particular combination was calculated by adding the weights of the coverslip, cell, thermal finish and substrate for 4 cm^2, plus the interconnects. In the case of the flexible array, (Variant 2 of Table 1), the weight of the thermal finish, interconnects and substrate amounted to 40 mg per cell. As Variant 1 was included only as a test of the adequacy of the flexible rear shield from the radiation viewpoint, it was not included in the power-to-weight estimates. The weight of the rigid substrate was assumed to be 1.6 kg m^{-2} [7] for both the shielding cases considered (Variants 3 and 4), giving, with the interconnects, a weight of 480 mg per cell.

Tables 6, 7 and 8 list the estimated equivalent 1MeV electron fluences, the resulting end-of-life powers at 62°C, (taken from Fig.20) and the specific masses for 125, 200 and 300μm cells respectively.

Fig.21, derived from these tables, shows power-to-weight ratio as a function of front cover thickness for the various coverslip/cell/rear shield combinations.

These power-to-weight ratios are, of course, for the solar panel only and take no account of the other elements of the array such as the stowage, deployment and support systems and the orientation and power transfer mechanisms. In flexible arrays, the panel weight constitutes a smaller proportion of the whole than is the case with rigid types, but the ratio of panel-to-total weight increases with size, whereas in rigid types it stays practically constant. Typical ratios in the case of a 1kW paddle[7] are 0.44 for the RAE flexible type and 0.63 for the rigid type.

7 DISCUSSION

7.1 Rigid array

Referring to Fig.21 it is apparent that:-

7.1.1 The solar panel power-to-weight ratio, p/w, is, in all cases considered, lower than that for the flexible array. Even when the p/w is adjusted to take account of the different structure weights for a 1kW array, the rigid type is still inferior to the flexible in this respect.

7.1.2 The assumption of infinite rear shielding (Variant 4) does not markedly improve the p/w ratio, even though the assumed substrate weight is unrealistically low.

7.1.3 The p/w ratio is almost insensitive to changes in the thickness of cell or coverslip, the substrate weight masking any advantages which might be gained from optimisation of cell or cover.

7.2 Flexible array

7.2.1 The panel p/w ratio increases as the coverslip thickness decreases, and this effect becomes more pronounced as the cell thickness decreases.

7.2.2 Various trades off exist between different coverslip/cell combinations. For example at p/w = 0.109 $W g^{-1}$, 25µm cover on a 300µm cell

$\equiv$ 150µm cover on a 200µm cell

$\equiv$ 235µm cover on a 125µm cell

and at p/w = 0.148 $W g^{-1}$ 25µm cover on a 200µm cell

$\equiv$ 120 m cover on a 125µm cell .

7.2.3 For covers less than 100 µm, a 125µm cell shows significant advantages. For example a 25µm cover on a 125µm cell has a p/w ratio of 0.2 $W g^{-1}$. The next best combination (no direct trade off being possible in this case) is either a 200µm cell with a 25µm cover, or a 125µm cell with a 100µm cover, for which the p/w ratio is 0.15 $W g^{-1}$. In a 1kW array this amounts to a weight penalty of about 2 kg, which could result in a further 2kg penalty, as the array mechanism would require strengthening to support the extra array weight.

8 CONCLUSIONS

In spite of the increased radiation received by the cell, higher p/w ratios are achieved by using the thinnest coverslip/cell/rear shield combinations.

The weight saving thus achieved is significant, and could amount to tens of kilograms for a multi-kilowatt array.

Rigid arrays bear a considerable weight penalty, even for moderate power levels. Moreover they offer no opportunity for the exploitation of thinner cells and coverslips.

For flexible arrays however, many options in coverslip and cell thickness are open, integral covers yielding the best p/w ratios. The thinnest discrete coverslips are 100μm thick, and it is doubtful whether thinner ones could be produced and mounted economically. Integral covers do not impose this difficulty as they are sputtered directly onto the cell. This also offers a wider choice of cell thickness which although increasing the p/w ratio, could reduce costs. It is possible that a 200μm cell with an integral 25μm cover could be the best choice for powers between a half and one kilowatt. For higher powers however, or for the same power where weight saving is paramount, the thinnest possible coverslip/cell combination should be used. Experience indicates that a 125μm cell with a 25-50μm cover will be quite fragile, but not impracticably so. Arrays of discrete 100μm covers on 125μm cells have already been successfully manufactured and qualified[8]. Such arrays are well supported against launch vibrations in the folded state and the only other hazard is the handling of the panels during integration, inspection, test and stowage operations. With refinements in these procedures, it should be feasible to construct and qualify folding flexible arrays of integrally covered 125μm cells.

Table 1

FRONT COVER, CELL AND REAR SHIELD VARIANTS

Coverslips

- 300 µm
- 150 µm
- 100 µm

} Discrete

- 75 µm
- 50 µm
- 25 µm

} Integral

Cells

- 300 µm
- 200 µm
- 125 µm

Rear shields

Variant No.	Components	Shielding mg cm^{-2}	Proportion of area	Effective shielding mg cm^{-2}
1	8 µm Cu (+ve contact of cell)	7.2	1	7.2
	50 µm Silastoseal B (thermal finish)	5.0	1	5.0
	TOTAL			12
2	8 µm Cu (+ve contact of cell)	7.2	1	7.2
	50µm Silastoseal B (thermal finish)	5.0	1	5.0
	50µm Kapton polyimide (substrate)	7.1	0.5	3.55
	25µm molybdenum (interconnect)	25.5	0.047	1.2
	TOTAL			17
3	8 µm Cu (+ve contact of cell)	7.2	1	7.2
	100µm Al (rigid substrate)	27.0	1	27.0
	TOTAL			34
4	Infinite rear shield	∞	1	∞

Table 2

BREAKDOWN OF EQUIVALENT 1MeV ELECTRON FLUX FOR FRONT INCIDENCE (cm^{-2} yr^{-1})

Damage source		Front cover thickness (μm)					
		25	50	75	100	150	300
Solar flare protons	1-10 MeV	1.26×10^{14}	6.47×10^{13}	5.25×10^{13}	3.83×10^{13}	1.94×10^{13}	0.68×10^{13}
	10-20 MeV	0.21×10^{13}	0.21×10^{13}	0.21×10^{13}	0.21×10^{13}	0.22×10^{13}	0.22×10^{13}
	20-100 MeV	0.08×10^{13}	0.08×10^{13}	0.08×10^{13}	0.08×10^{13}	0.08×10^{13}	0.08×10^{13}
	TOTAL	1.29×10^{14}	6.76×10^{13}	5.54×10^{13}	4.12×10^{13}	2.24×10^{13}	1.0×10^{13}
Trapped electrons		7.54×10^{13}	7.09×10^{13}	6.70×10^{13}	6.16×10^{13}	5.65×10^{13}	4.25×10^{13}

Table 3

BREAKDOWN OF EQUIVALENT 1MeV ELECTRON FLUENCE FOR REAR INCIDENCE (cm^{-2} yr^{-1})

Cell thickness (μm)	Damage source		Rear shielding (mg cm^{-2})		
			12	17	34
125	Solar flare protons	1-10 MeV	1.61×10^{14}	6.82×10^{13}	4.38×10^{13}
		10-20 MeV	0.21×10^{13}	0.21×10^{13}	0.21×10^{13}
		20-100 MeV	0.08×10^{13}	0.08×10^{13}	0.08×10^{13}
		TOTAL	1.64×10^{14}	7.11×10^{13}	4.67×10^{13}
200	Solar flare protons	1-10 MeV	1.36×10^{14}	6.42×10^{13}	4.21×10^{13}
		10-20 MeV	0.21×10^{13}	0.21×10^{13}	0.21×10^{13}
		20-100 MeV	0.08×10^{13}	0.08×10^{13}	0.08×10^{13}
		TOTAL	1.39×10^{14}	6.71×10^{13}	4.50×10^{13}
300	Solar flare proton	1-10 MeV	1.08×10^{14}	5.19×10^{13}	2.92×10^{13}
		10-20 MeV	0.21×10^{13}	0.21×10^{13}	0.21×10^{13}
		20-100 MeV	0.08×10^{13}	0.08×10^{13}	0.08×10^{13}
		TOTAL	1.11×10^{14}	5.48×10^{13}	3.21×10^{13}
125 200 300	Trapped electrons		6.82×10^{13}	6.41×10^{13}	5.38×10^{13}

Table 4

ANNUAL EQUIVALENT 1MeV ELECTRON FLUENCE FROM SOLAR FLARE PROTONS ONLY, FRONT AND REAR INCIDENCE, DURING PERIOD 1975-77 (cm^{-2} yr^{-1})

Cell thickness (μm)	Rear shielding (mg cm^{-2})	Front cover thickness (μm)					
		25	50	75	100	150	300
125	12	2.9×10^{14}	2.3×10^{14}	2.2×10^{14}	2.1×10^{14}	1.9×10^{14}	1.7×10^{14}
	17	2.0×10^{14}	1.4×10^{14}	1.3×10^{14}	1.1×10^{14}	9.3×10^{13}	8.1×10^{13}
	34	1.8×10^{14}	1.1×10^{14}	1.0×10^{14}	8.9×10^{13}	6.9×10^{13}	5.7×10^{13}
200	12	2.7×10^{14}	2.1×10^{14}	1.9×10^{14}	1.8×10^{14}	1.6×10^{14}	1.5×10^{14}
	17	2.0×10^{14}	1.3×10^{14}	1.2×10^{14}	1.1×10^{14}	8.9×10^{13}	7.7×10^{13}
	34	1.7×10^{14}	1.1×10^{14}	1.0×10^{14}	8.6×10^{13}	7.7×10^{13}	5.5×10^{13}
300	12	2.4×10^{14}	1.8×10^{14}	1.7×10^{14}	1.3×10^{14}	1.3×10^{14}	1.2×10^{14}
	17	1.8×10^{14}	1.2×10^{14}	1.1×10^{14}	7.7×10^{13}	7.7×10^{13}	6.5×10^{13}
	34	1.6×10^{14}	1.0×10^{14}	8.8×10^{13}	5.4×10^{13}	5.4×10^{13}	4.2×10^{13}
125 200 300	Infinite	1.3×10^{14}	6.8×10^{13}	5.5×10^{13}	4.1×10^{13}	2.2×10^{13}	1.0×10^{13}

Table 5

EQUIVALENT 1MeV ELECTRON FLUENCE FROM SOLAR FLARE PROTONS AND TRAPPED ELECTRONS, FRONT AND REAR INCIDENCE, FOR PERIOD 1975-80

Cell thickness (μm)	Rear shielding (mg cm^{-2})	Front cover thickness (μm)					
		25	50	75	100	150	300
125	12	3.6×10^{15}	3.0×10^{15}	2.9×10^{15}	2.7×10^{15}	2.5×10^{15}	2.3×10^{15}
	17	2.7×10^{15}	2.1×10^{15}	2.0×10^{15}	1.7×10^{15}	1.5×10^{15}	1.3×10^{15}
	34	2.4×10^{15}	1.7×10^{15}	1.6×10^{15}	1.5×10^{15}	1.2×10^{15}	1.0×10^{15}
200	12	3.4×10^{15}	2.8×10^{15}	2.6×10^{15}	2.4×10^{15}	2.2×10^{15}	2.1×10^{15}
	17	2.7×10^{15}	2.0×10^{15}	1.9×10^{15}	1.7×10^{15}	1.5×10^{15}	1.3×10^{15}
	34	2.3×10^{15}	1.7×10^{15}	1.6×10^{15}	1.4×10^{15}	1.3×10^{15}	1.1×10^{15}
300	12	3.1×10^{15}	2.5×10^{15}	2.4×10^{15}	2.1×10^{15}	1.9×10^{15}	1.8×10^{15}
	17	2.5×10^{15}	1.9×10^{15}	1.8×10^{15}	1.6×10^{15}	1.4×10^{15}	1.2×10^{15}
	34	2.2×10^{15}	1.6×10^{15}	1.5×10^{15}	1.3×10^{15}	1.1×10^{15}	0.9×10^{15}
125 200 300	Infinite	1.7×10^{15}	1.0×10^{15}	0.9×10^{15}	0.7×10^{15}	0.5×10^{15}	0.3×10^{15}

Table 6

SUMMARY OF ESTIMATES, 125μm CELL

Array type	Parameter		Front cover (μm)					
			25	50	75	100	150	300
Flexible	Equivalent 1MeV electron fluence 1975-80 (cm^{-2})		2.7×10^{15}	2.0×10^{15}	1.9×10^{15}	1.7×10^{15}	1.5×10^{15}	1.3×10^{15}
	End of life maximum power at 62°C (mW)		37.3	38.8	39.0	39.5	40.1	40.7
	Specific mass of solar panel (g/cell)		0.182	0.205	0.228	0.251	0.298	0.437
Rigid	Equivalent 1MeV electron fluence 1975-80 (cm^{-2})	100μm Al. rear shielding	2.4×10^{15}	1.7×10^{15}	1.6×10^{15}	1.5×10^{15}	1.2×10^{15}	1.0×10^{15}
		Infinite rear shielding	1.7×10^{15}	1.0×10^{15}	0.9×10^{15}	0.7×10^{15}	0.5×10^{15}	0.3×10^{15}
	End of life maximum power at 62°C (mW)	100μm Al. rear shielding	37.8	39.5	39.9	40.1	41.0	41.8
		Infinite rear shielding	39.5	41.8	42.1	43.0	43.9	45.0
	Specific mass of solar panel (g/cell)		0.622	0.645	0.668	0.691	0.738	0.877

Table 7

SUMMARY OF ESTIMATES, 200μm CELL

Array type	Parameter		Front cover (μm)					
			25	50	75	100	150	300
Flexible	Equivalent 1MeV electron fluence 1975-80 (cm^{-2})		2.7×10^{15}	2.0×10^{15}	1.9×10^{15}	1.7×10^{15}	1.5×10^{15}	1.3×10^{15}
	End of life maximum power at 62°C (mW)		37.3	38.8	39.0	39.5	40.1	40.7
	Specific mass of solar panel (g/cell)		0.253	0.276	0.300	0.323	0.369	0.508
Rigid	Equivalent 1MeV electron fluence, 1975-80 (cm^{-2})	100μm Al. rear shielding	2.3×10^{15}	1.7×10^{15}	1.6×10^{15}	1.4×10^{15}	1.3×10^{15}	1.1×10^{15}
		Infinite rear shielding	1.7×10^{15}	1.0×10^{15}	0.9×10^{15}	0.7×10^{15}	0.5×10^{15}	0.3×10^{15}
	End of life maximum power at 62°C (mW)	100μm Al. rear shielding	38.1	39.5	39.9	40.2	40.7	41.4
		Infinite rear shielding	39.5	41.8	42.1	43.0	43.9	45.0
	Specific mass of solar panel (g/cell)		0.693	0.716	0.740	0.763	0.809	0.948

Table 8

SUMMARY OF ESTIMATES, 300μm CELL

Array type	Parameter		Front cover (μm)					
			25	50	75	100	150	300
Flexible	Equivalent 1MeV electron fluence, 1975-80 (cm^{-2})		2.5×10^{15}	1.9×10^{15}	1.8×10^{15}	1.6×10^{15}	1.4×10^{15}	1.2×10^{15}
	End of life maximum power at 62°C (mW)		37.7	39.0	39.3	39.9	40.2	41.0
	Specific mass of solar panel (g/cell)		0.347	0.370	0.394	0.417	0.463	0.602
Rigid	Equivalent 1 MeV electron fluence, 1975-80 (cm^{-2})	100μm Al. rear shielding	2.2×10^{15}	1.6×10^{15}	1.5×10^{15}	1.3×10^{15}	1.1×10^{15}	0.9×10^{15}
		Infinite rear shielding	1.7×10^{15}	1.0×10^{15}	0.9×10^{15}	0.7×10^{15}	0.5×10^{15}	0.3×10^{15}
	End of life maximum power at 62°C (mW)	100μm Al. rear shielding	38.4	39.9	40.1	40.7	41.4	42.1
		Infinite rear shielding	39.5	41.8	42.1	43.0	43.9	45.0
	Specific mass of solar panel (g/cell)		0.787	0.810	0.834	0.857	0.903	1.042

REFERENCES

No.	Author	Title, etc.
1	-	Canadian Department of Communications Requirement - Spacecraft Environmental Design and Test Document. Ref. No. EV01-01 (1972)
2	-	NASA TMX 53865, 2nd edition, August, 1970
3	G. Brackley K. Lawson D.W. Satchell	Integral covers for silicon solar cells. 9th IEEE Photovoltaic Specialists Conference. Silver Spring, Md., USA, May 1972
4	F.C. Treble	Status report on RAE advanced lightweight solar array development. RAE Technical Report 72109 (1972)
5	F.C. Treble M.W. Walkden A.F. Dunnet C. Whitehead (AWEE)	Proton damage in silicon solar cells - final report prepared for Communications Satellite Corporation. Washington, DC, USA, Contract CSC-SS-183, July 1971
6	R.L. Crabb M.W. Walkden	Energy dependence of electron damage in silicon solar cells. RAE Technical Report 68139 (1968)
7	F.C. Treble	Solar arrays for the next generation of communication satellites. RAE Technical Memorandum Space 185 (1972)
8	A.A. Dollery A.F. Dunnet N.S. Reed	Qualification of 280W lightweight solar array. RAE Technical Report (to be published)

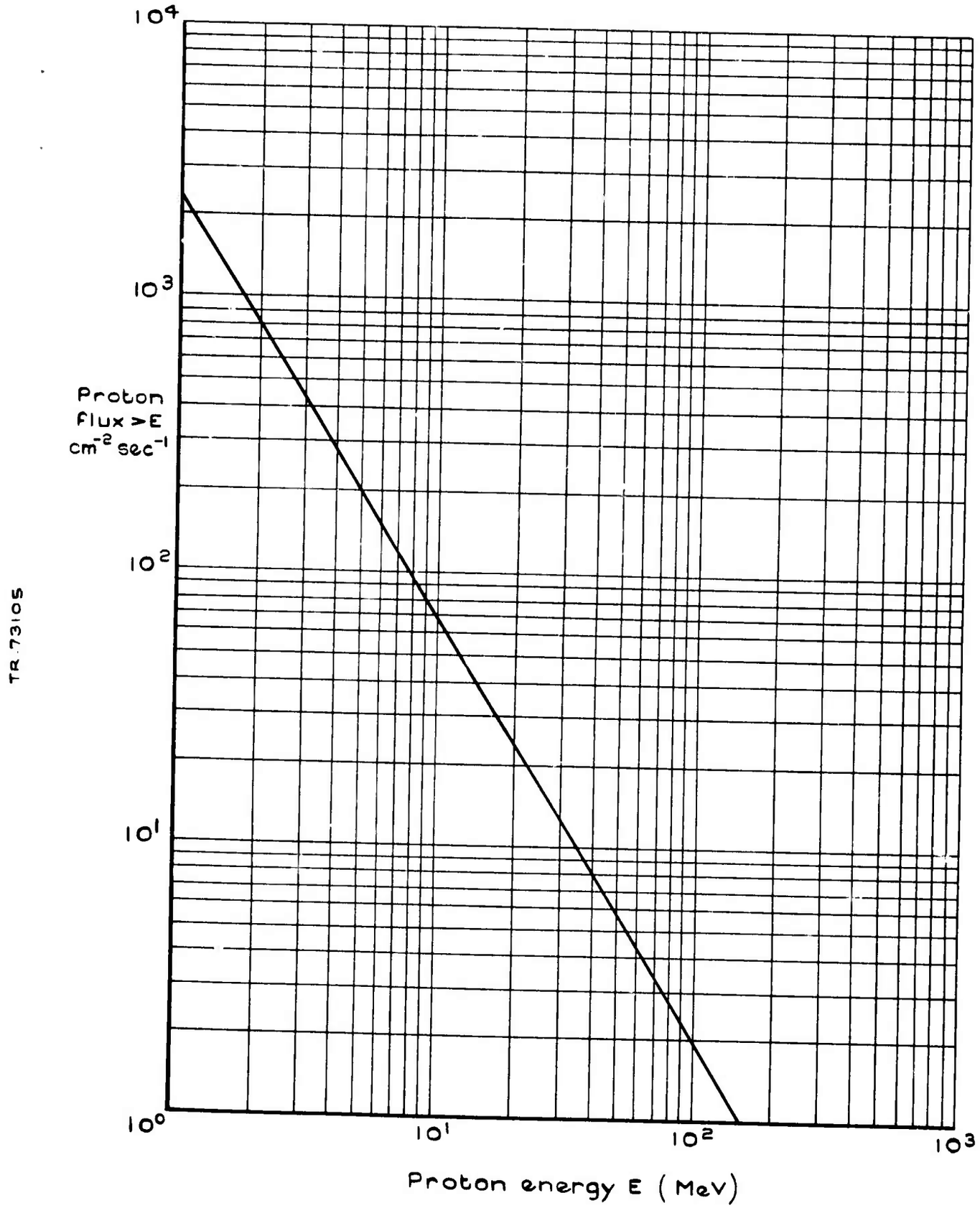

Fig. 1 Integrated low energy proton flux (>E)
1975-77

Fig.2

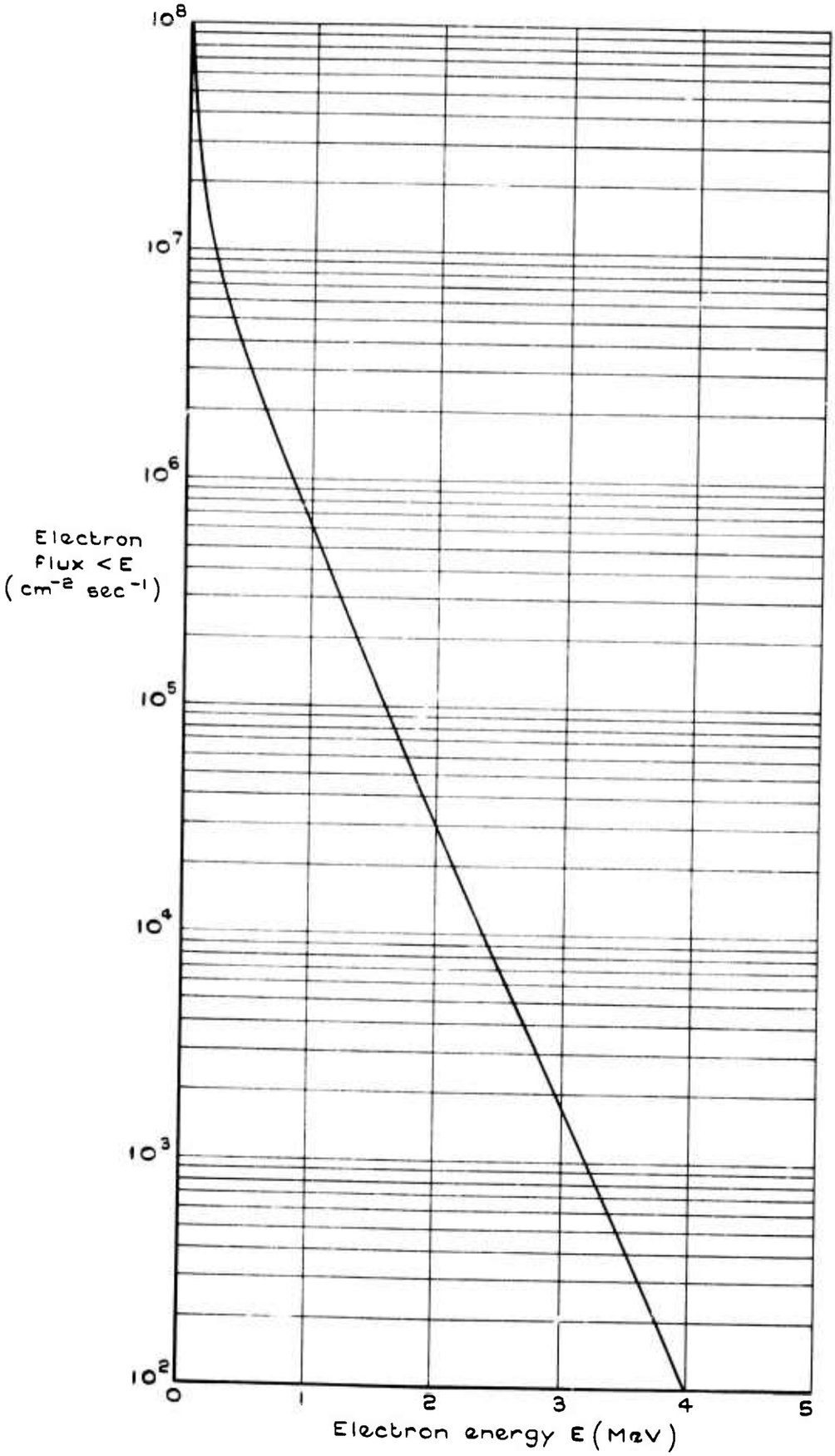

TR73105

Fig.2 Time averaged integral electron flux ϕ (>E) (1975-77)

Fig. 3

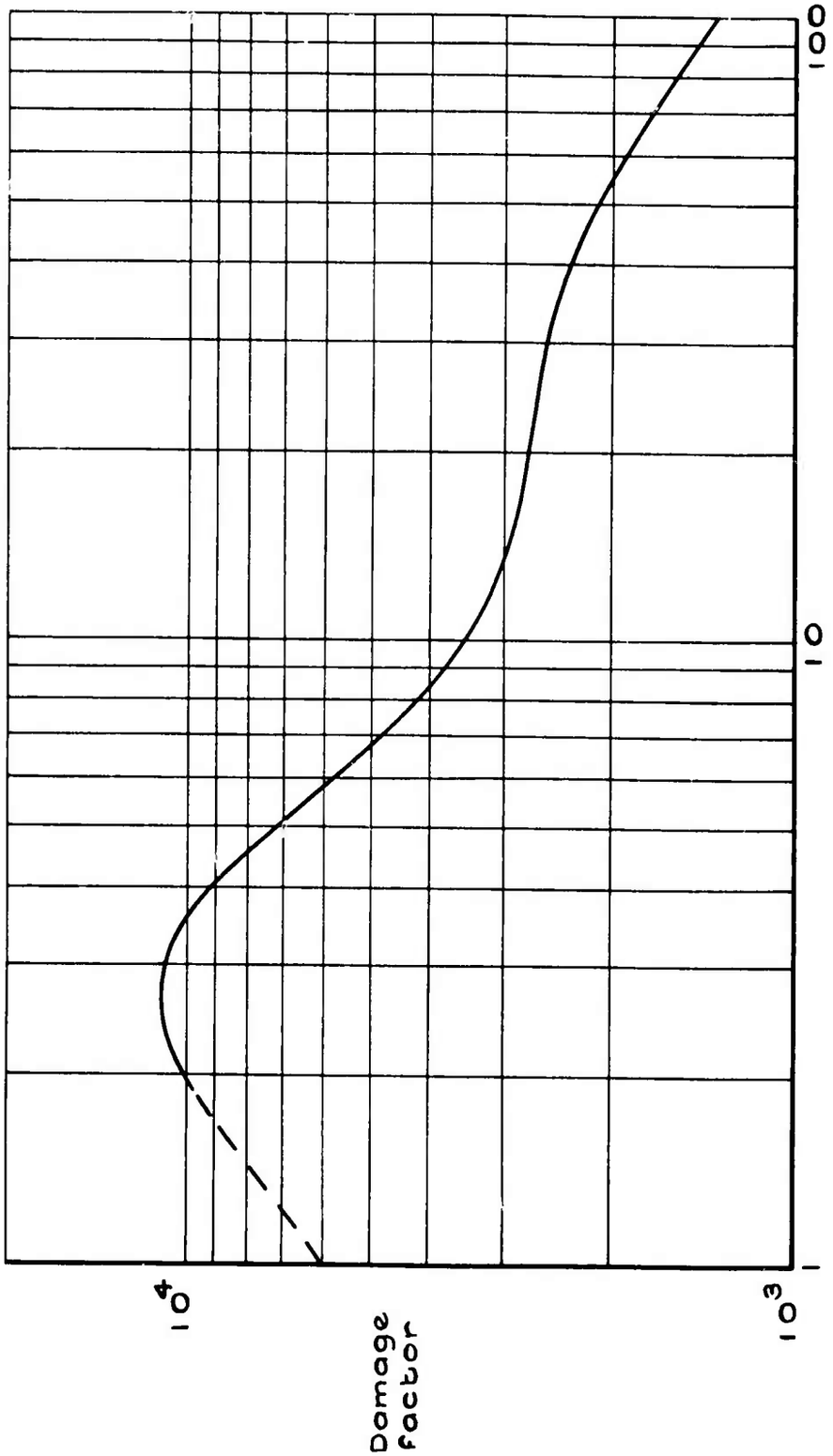

Fig.3 Front incidence proton damage factors for uncovered cells

T.R.73105

Fig. 4

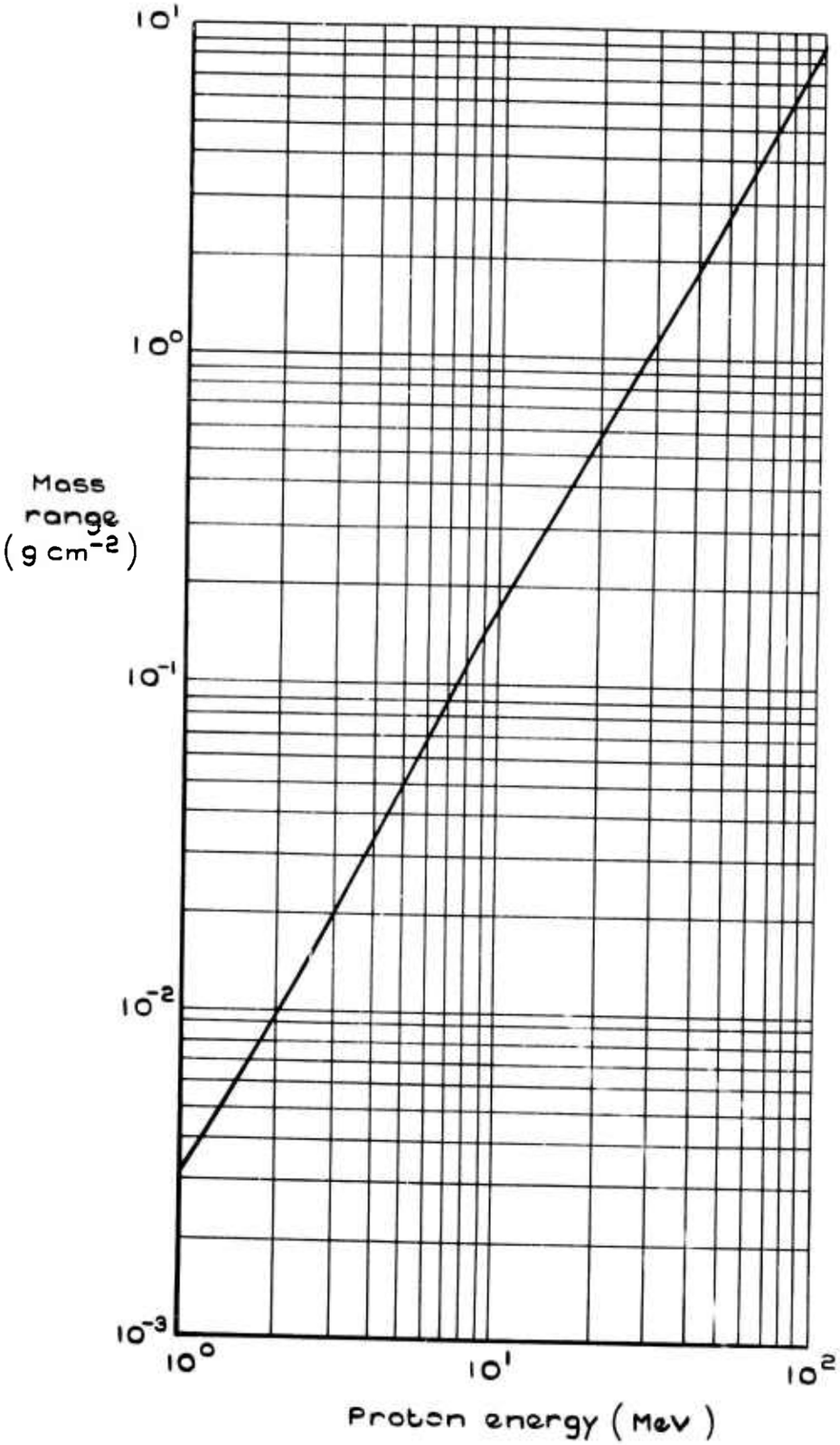

T.A.73105

Fig. 4 Mass-range of protons in SiO_2

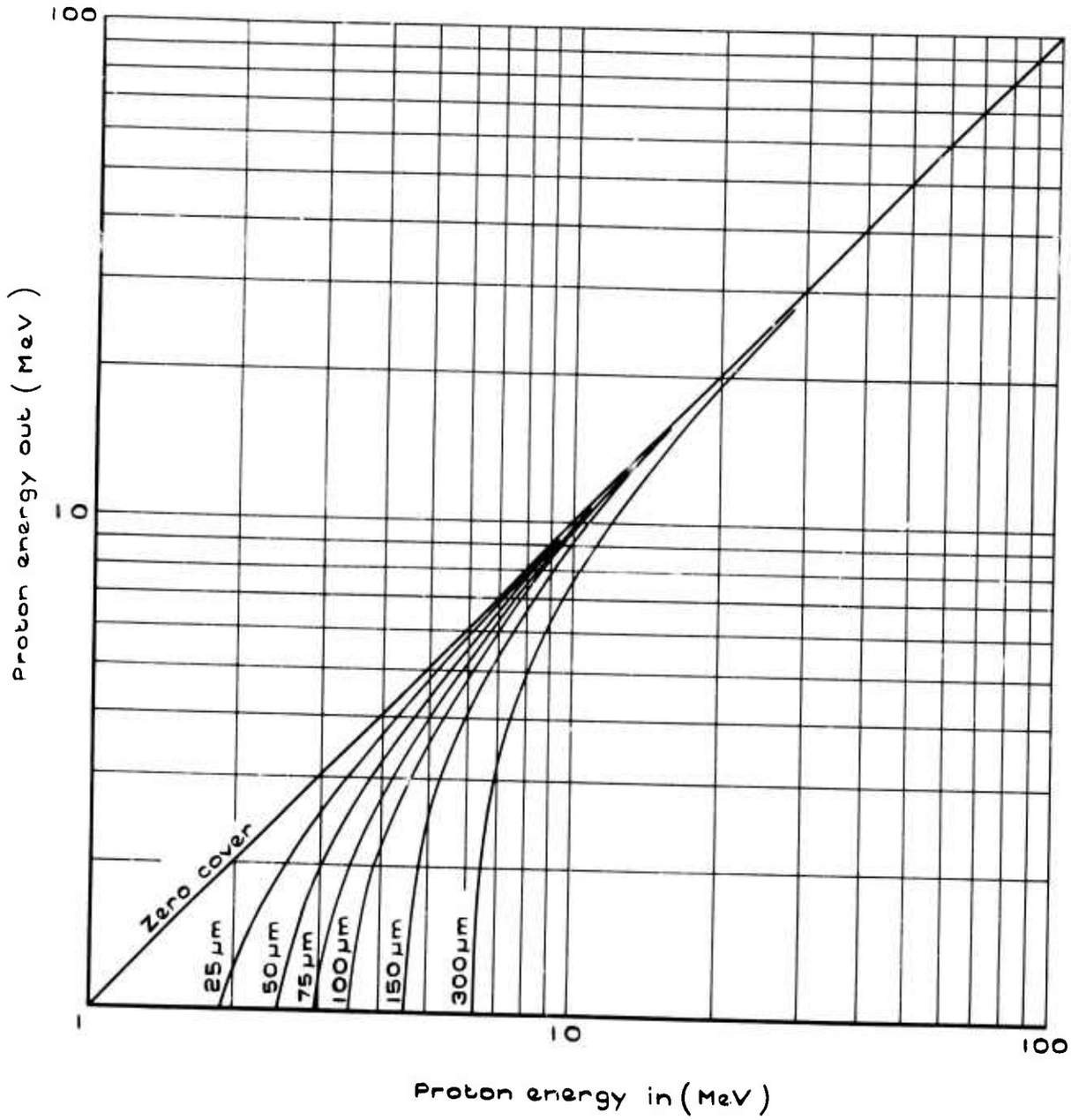

TR 73105

Fig.5 Exit versus incident energy for protons in SiO_2 covers

Fig. 7

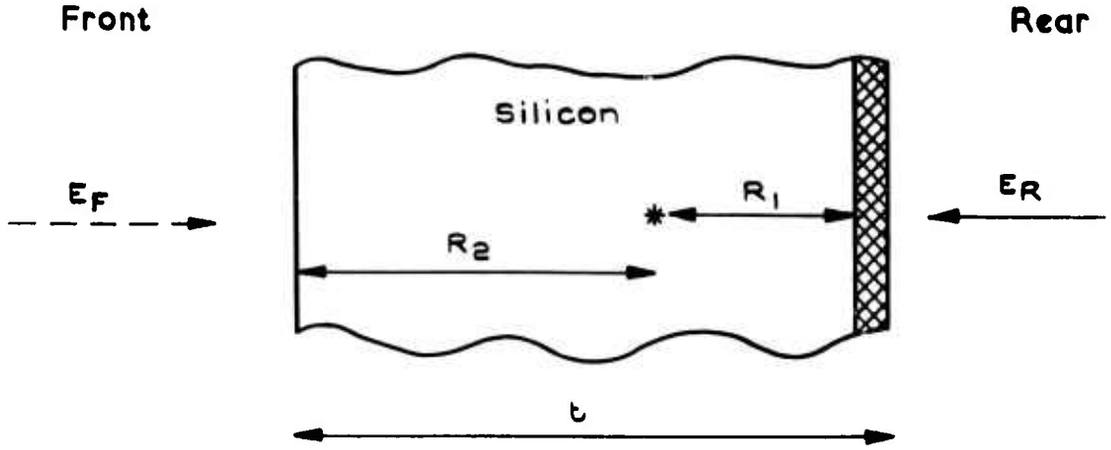

E_R = Energy of proton incident on rear shield
R_1 = Range in silicon after attenuation of rear shield
t = Cell thickness
R_2 = Distance from front surface
E_F = Equivalent front incidence energy
K = Damage factor for E_F

T.R.73.103

1

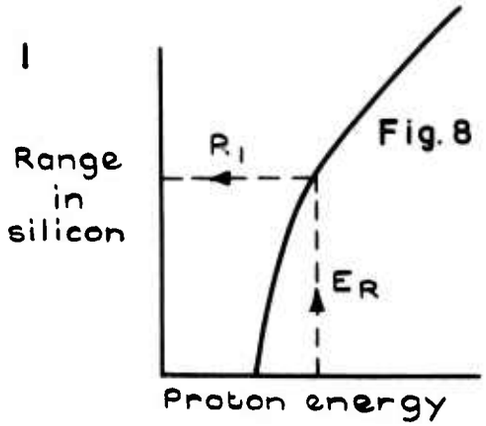

Fig. 8

2

$$R_2 = t - R_1$$

3

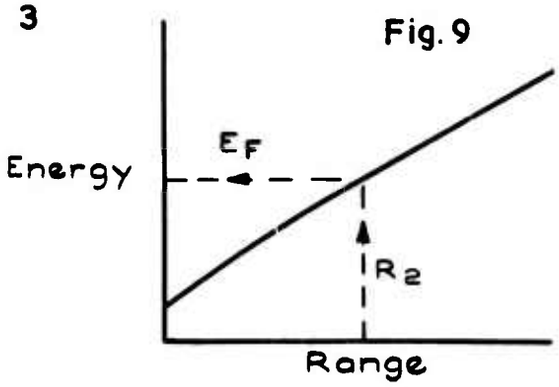

Fig. 9

4

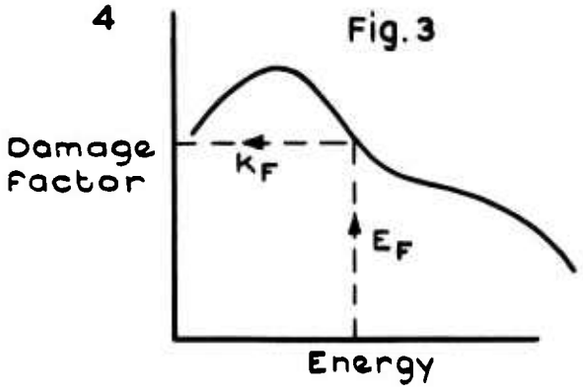

Fig. 3

5

$$K_R \equiv K_F$$

Fig. 7 Determination of rear incidence damage factors

Fig.8

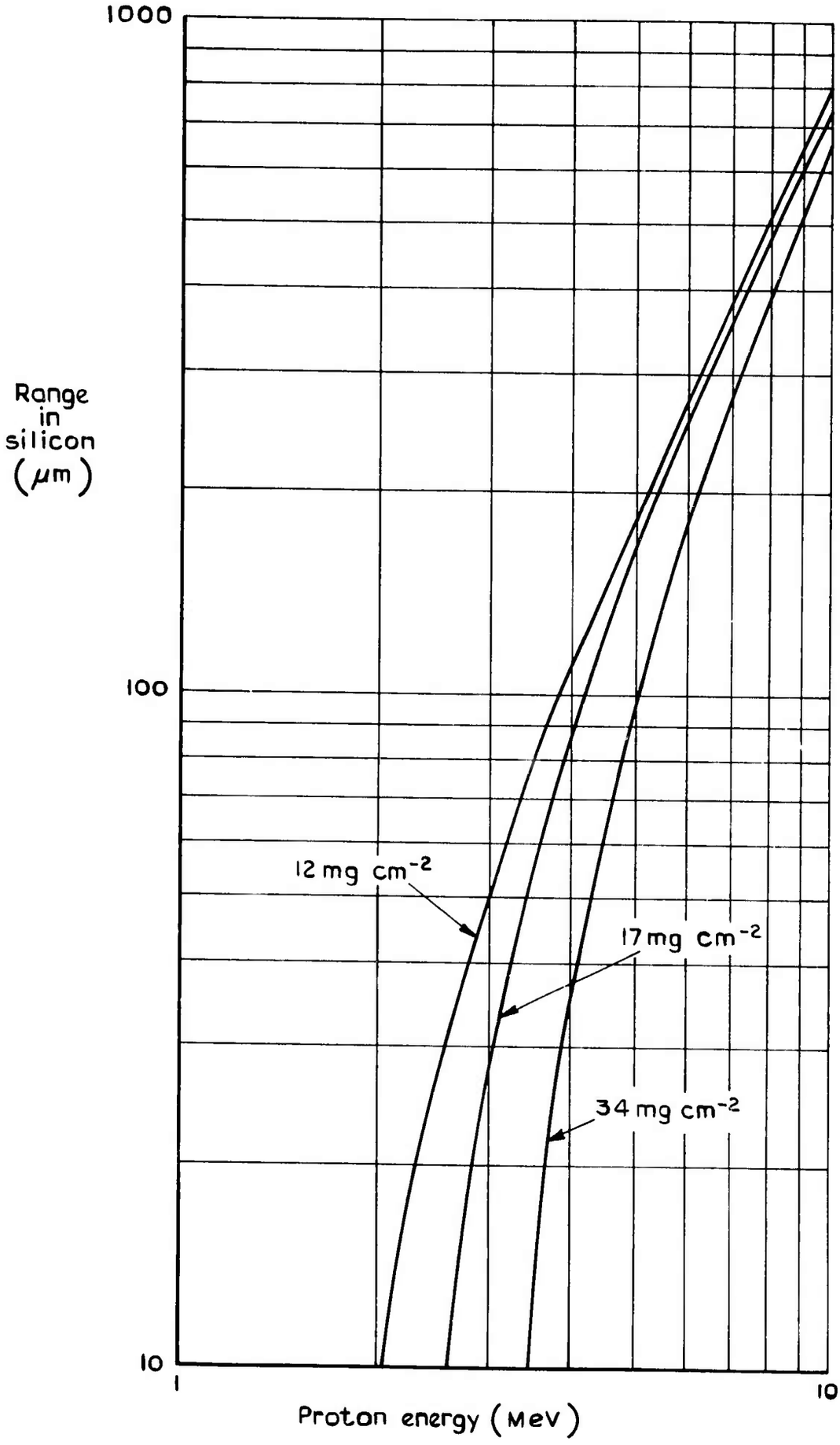

T.R. 73105

Fig.8 Range of protons in silicon after passing through rear shields

Fig. 9

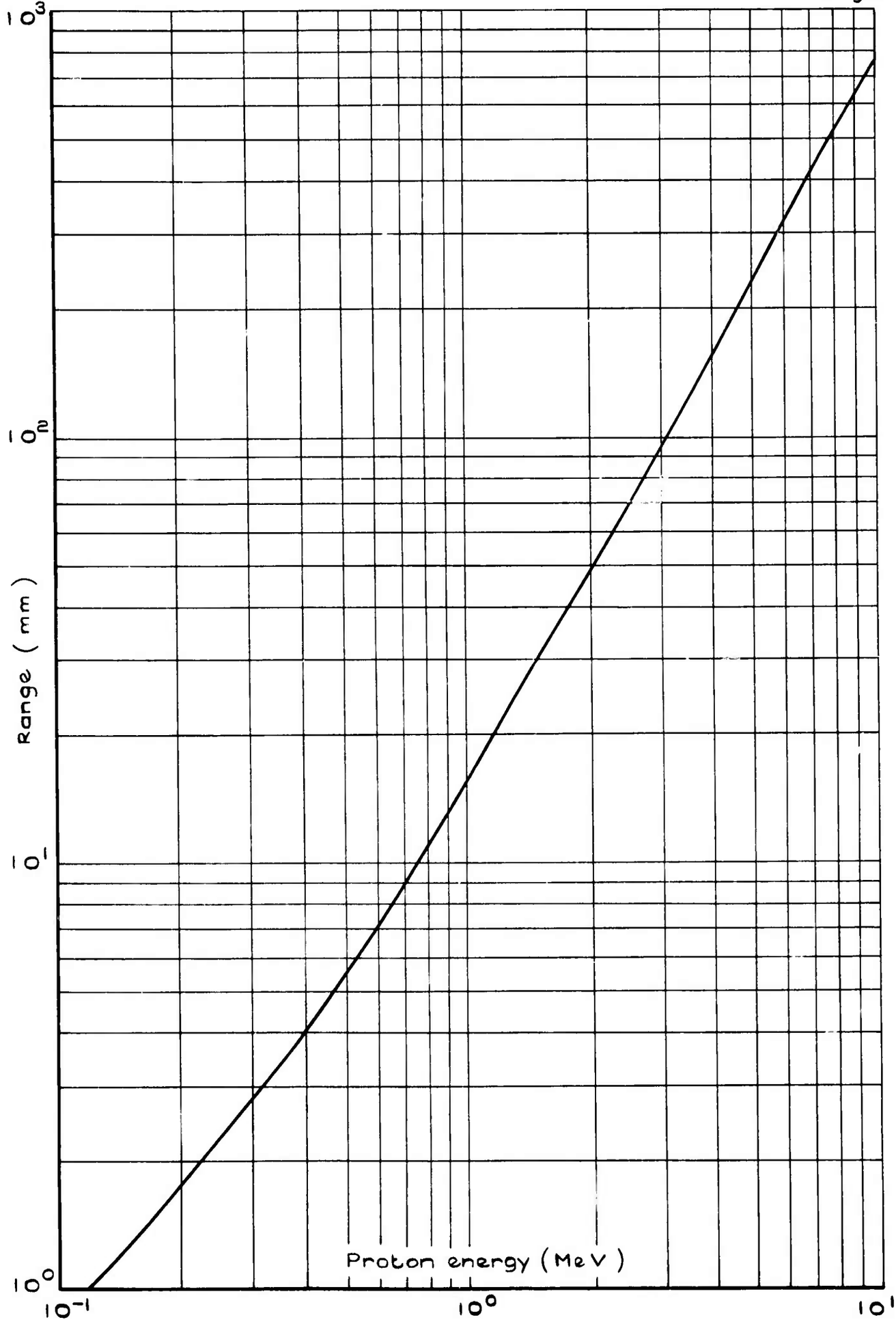

T.R.7310S

Fig.9 Range of protons in silicon

Fig. 10

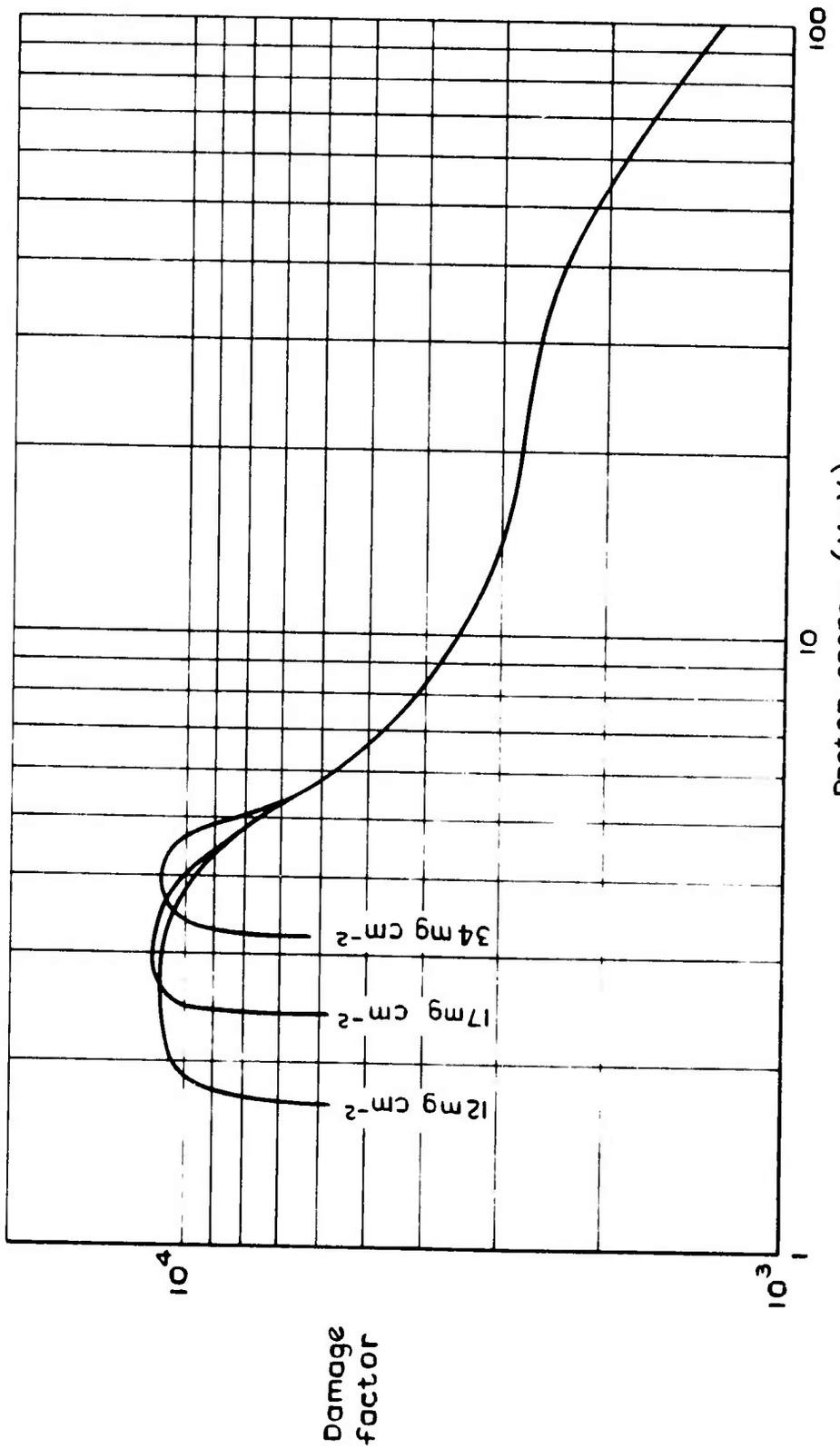

Fig.10 Rear incidence proton damage factors for 125μm cells and 3 different rear shields

TR 73105

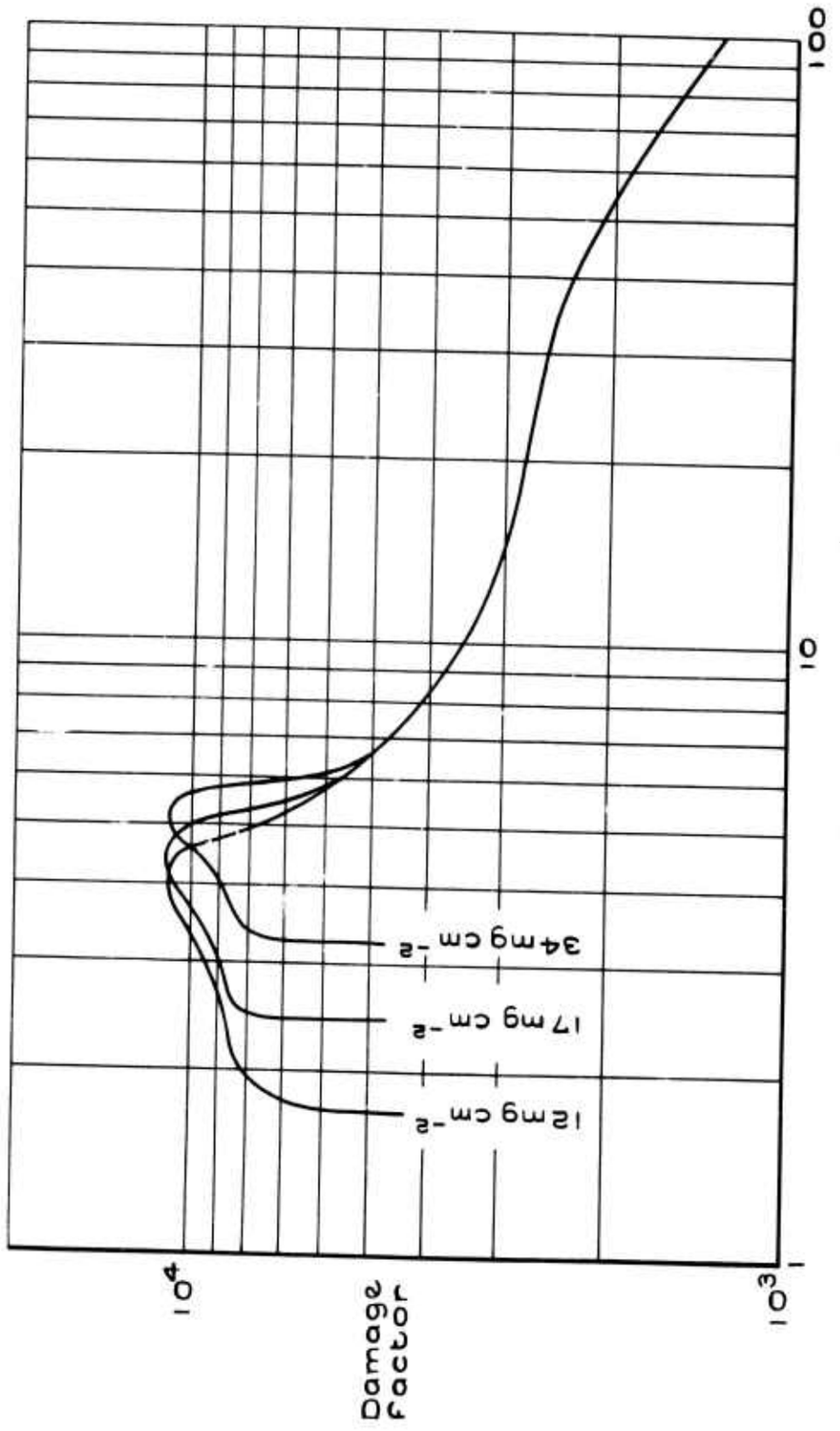

Fig.11 Rear incidence proton damage factors for 200μm cells and 3 different rear shields

Fig.12

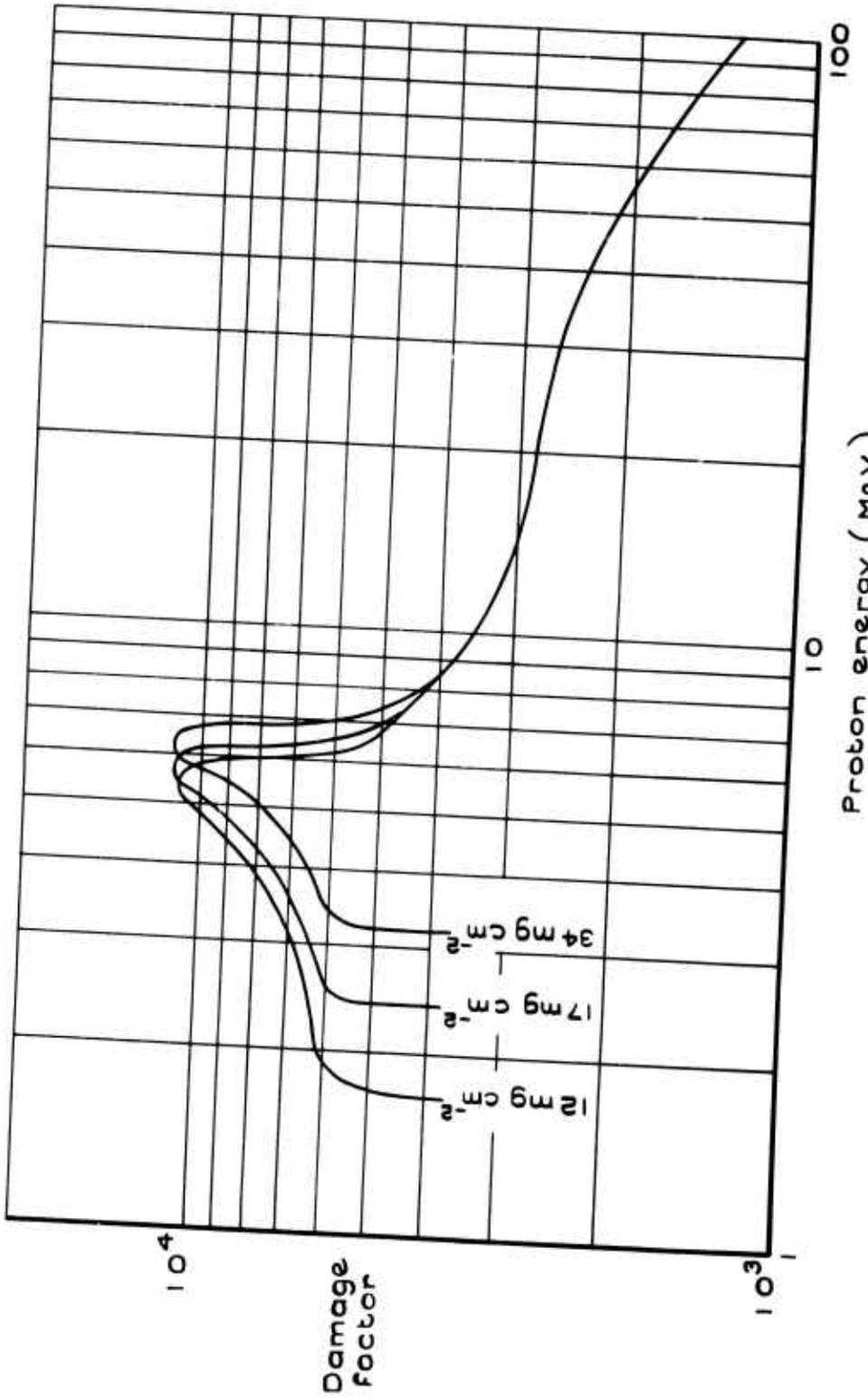

Fig.12 Rear incidence proton damage factors for 300μm cells and 3 different rear shields

T.R.73105

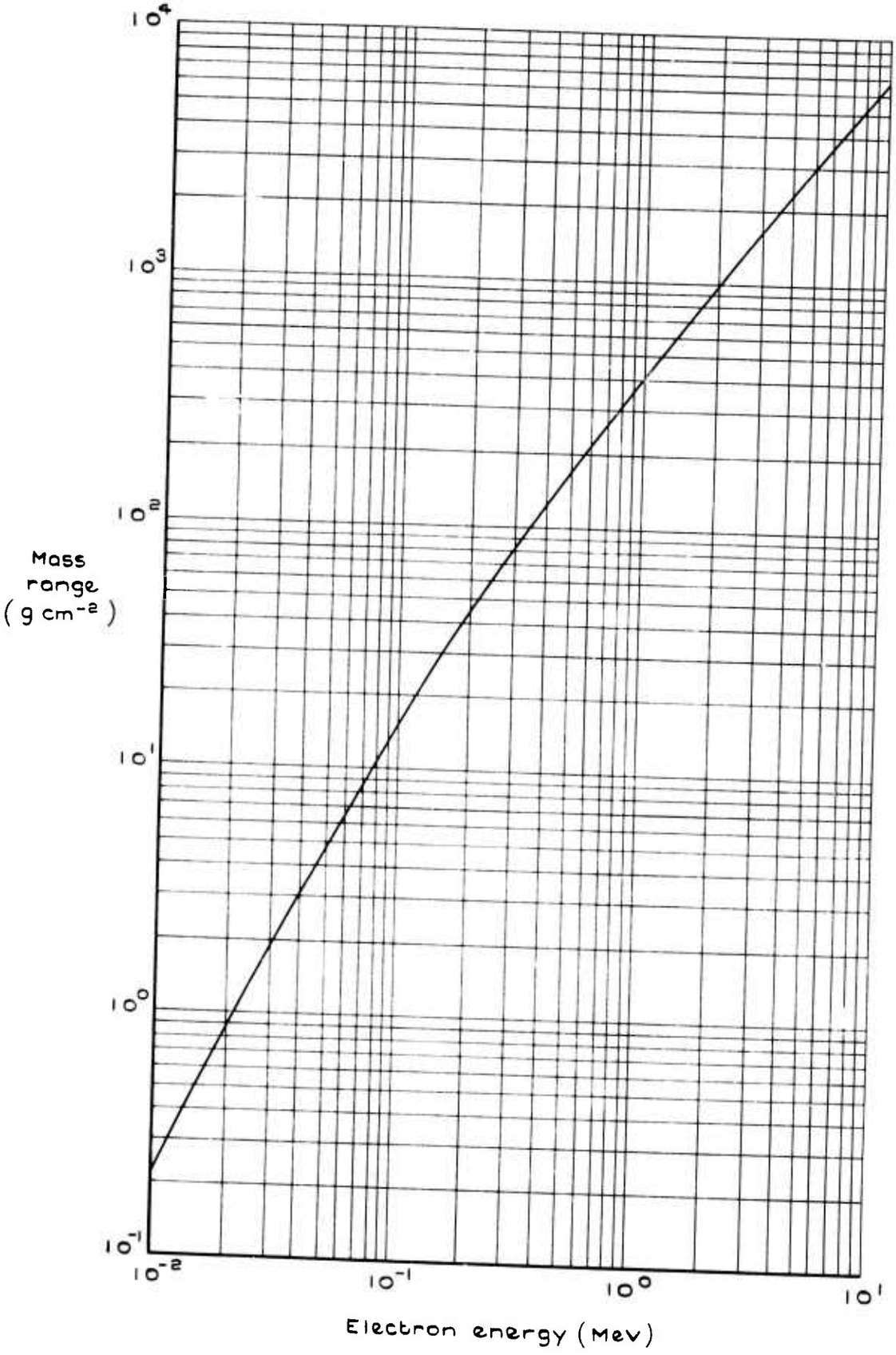

TA.7305

Fig.13 Mass range of electrons in SiO_2

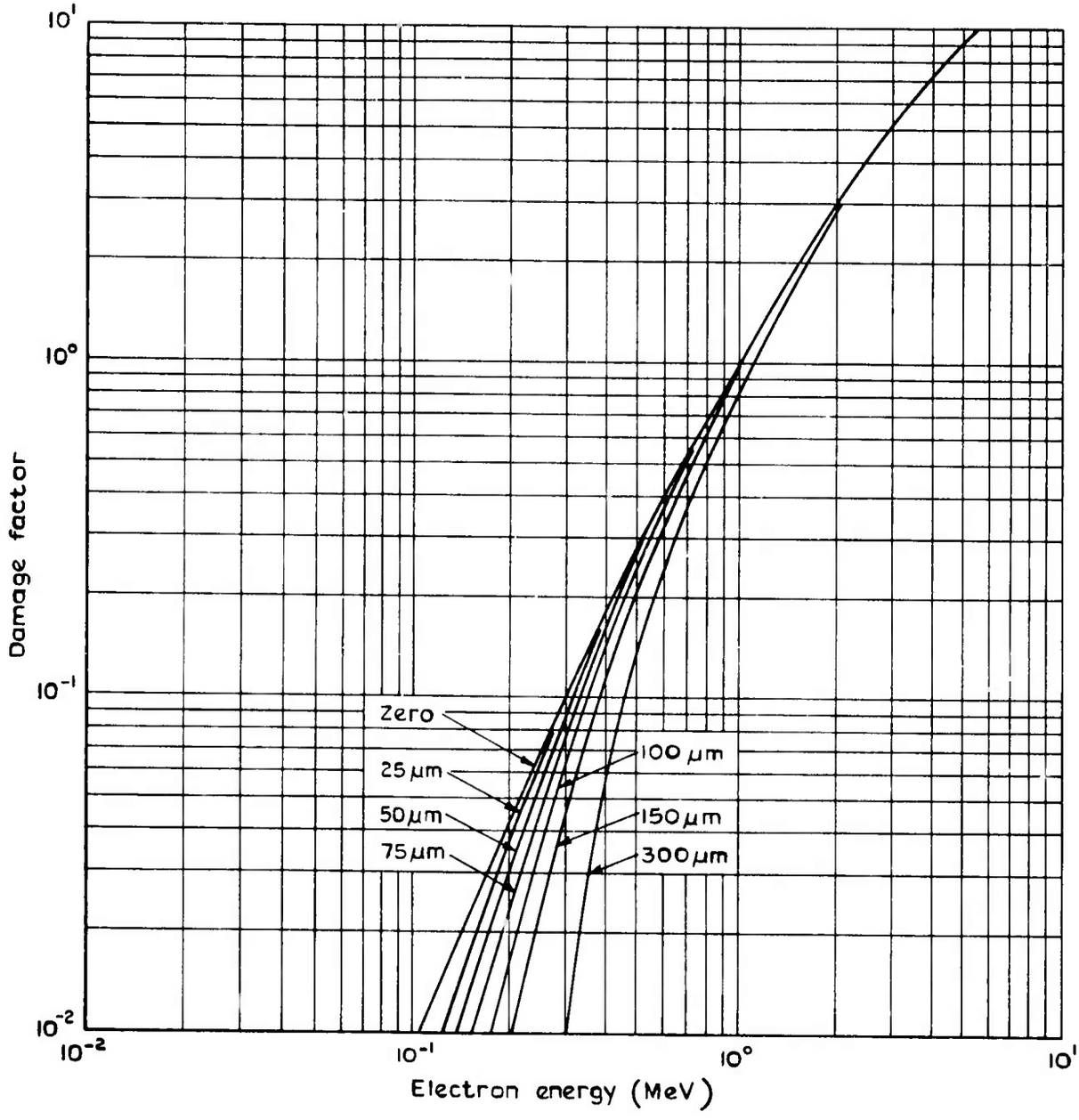

Fig.15 Effect of front cover thickness on electron damage factors

Fig.16

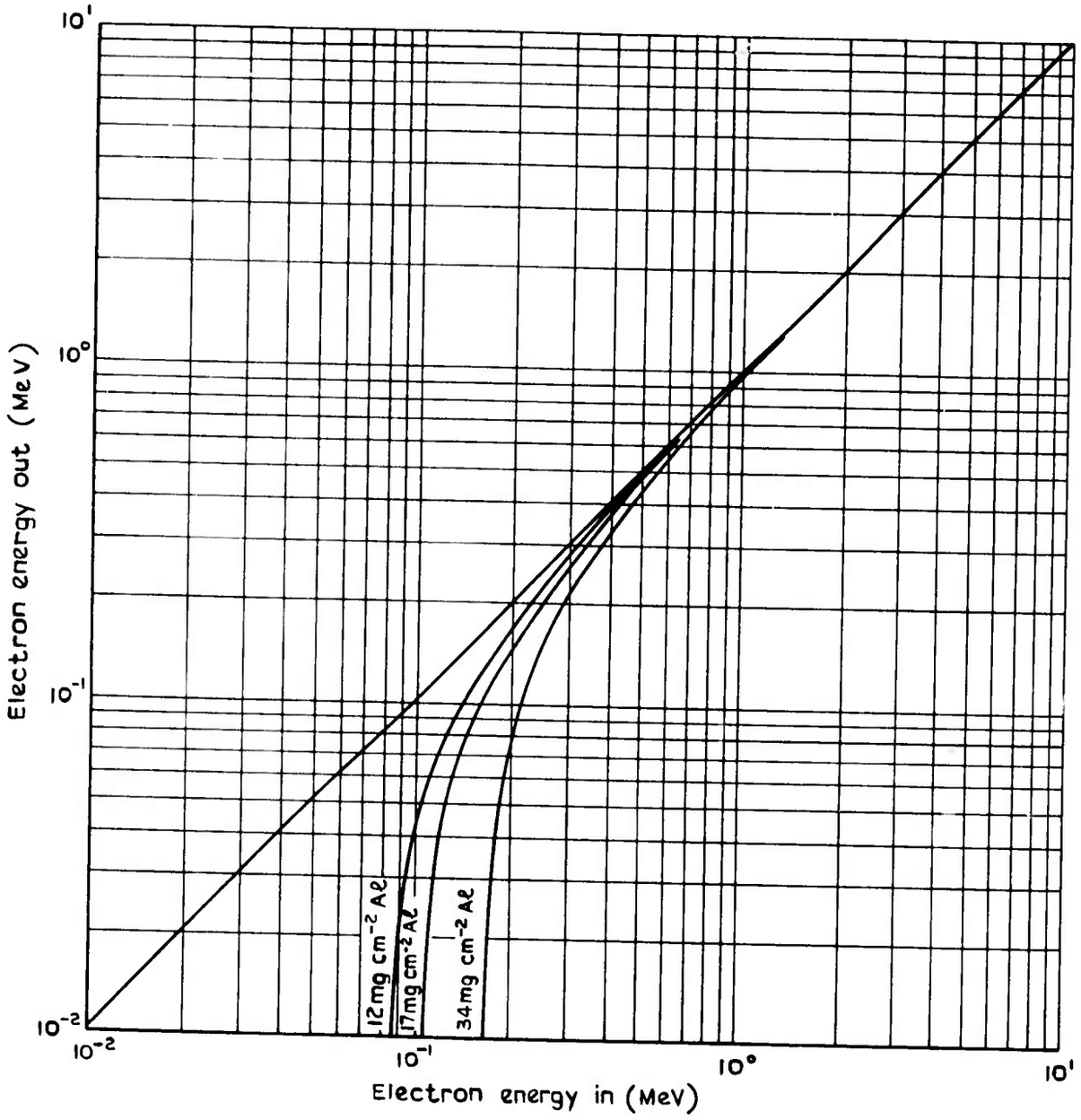

T.R.73105

Fig.16 Exit versus incident energy for rear electrons in 3 rear shields

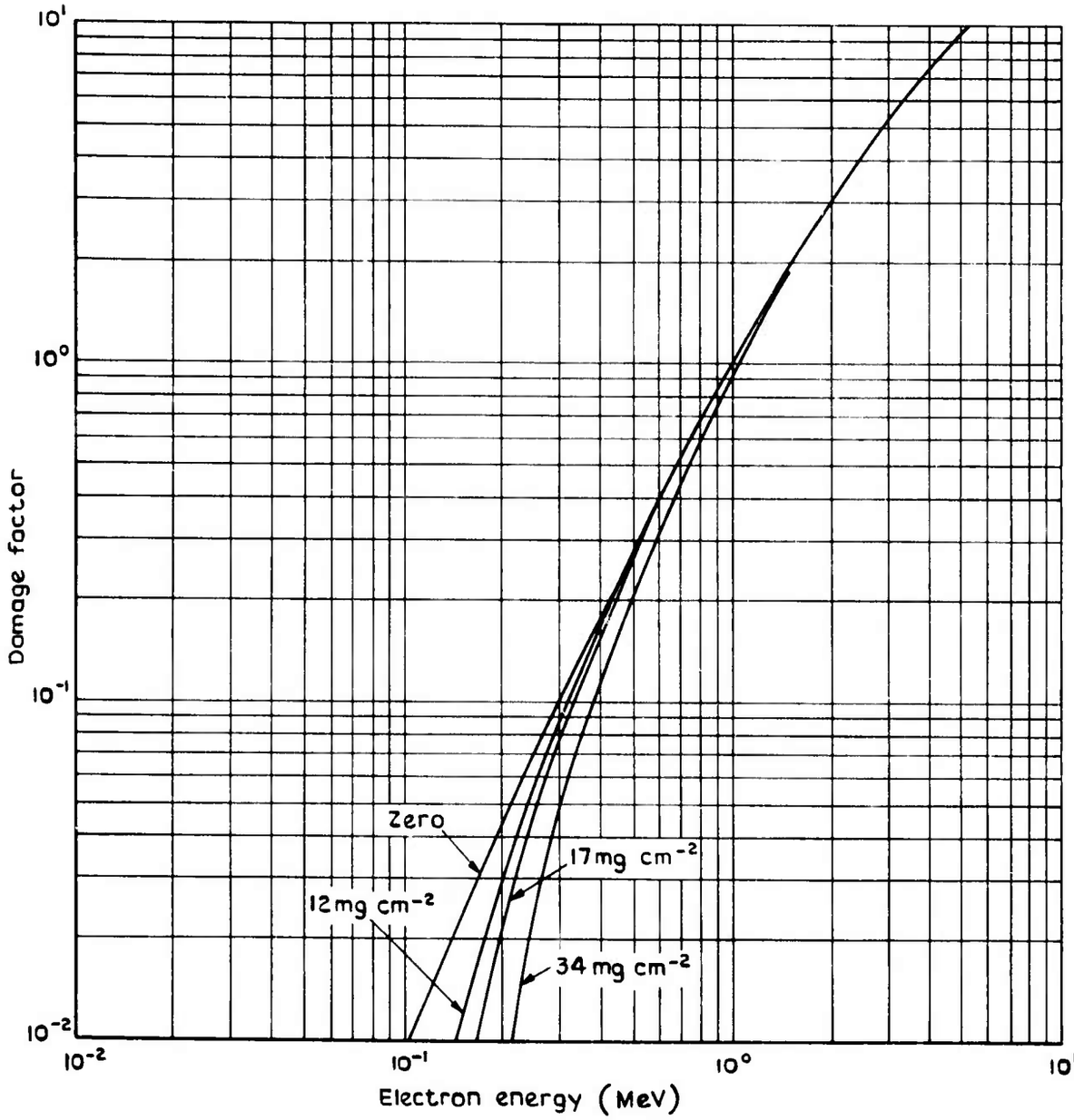

T.R. 73105

Fig.17 Effect of rear shielding on electron damage factors

Fig.18

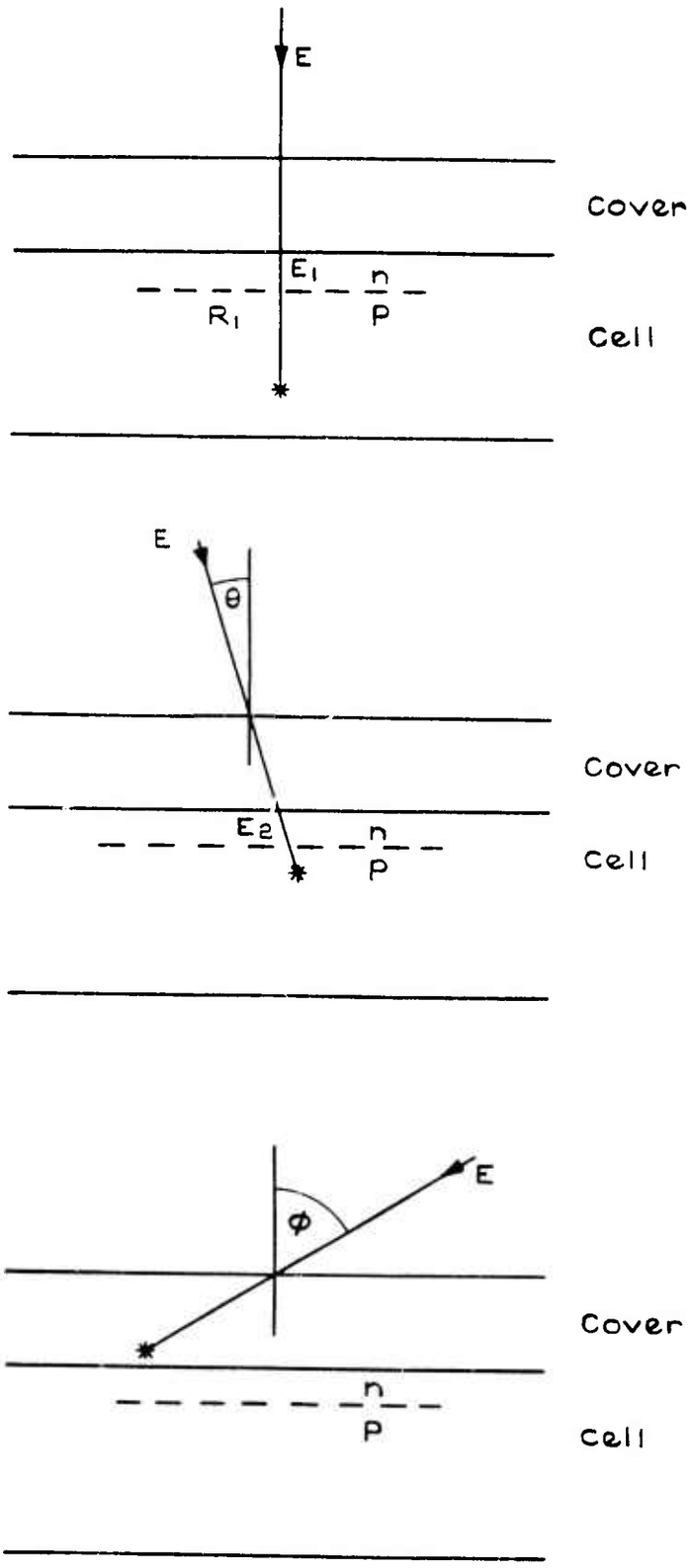

TR 73105

Fig.18 Effect of proton angle of incidence

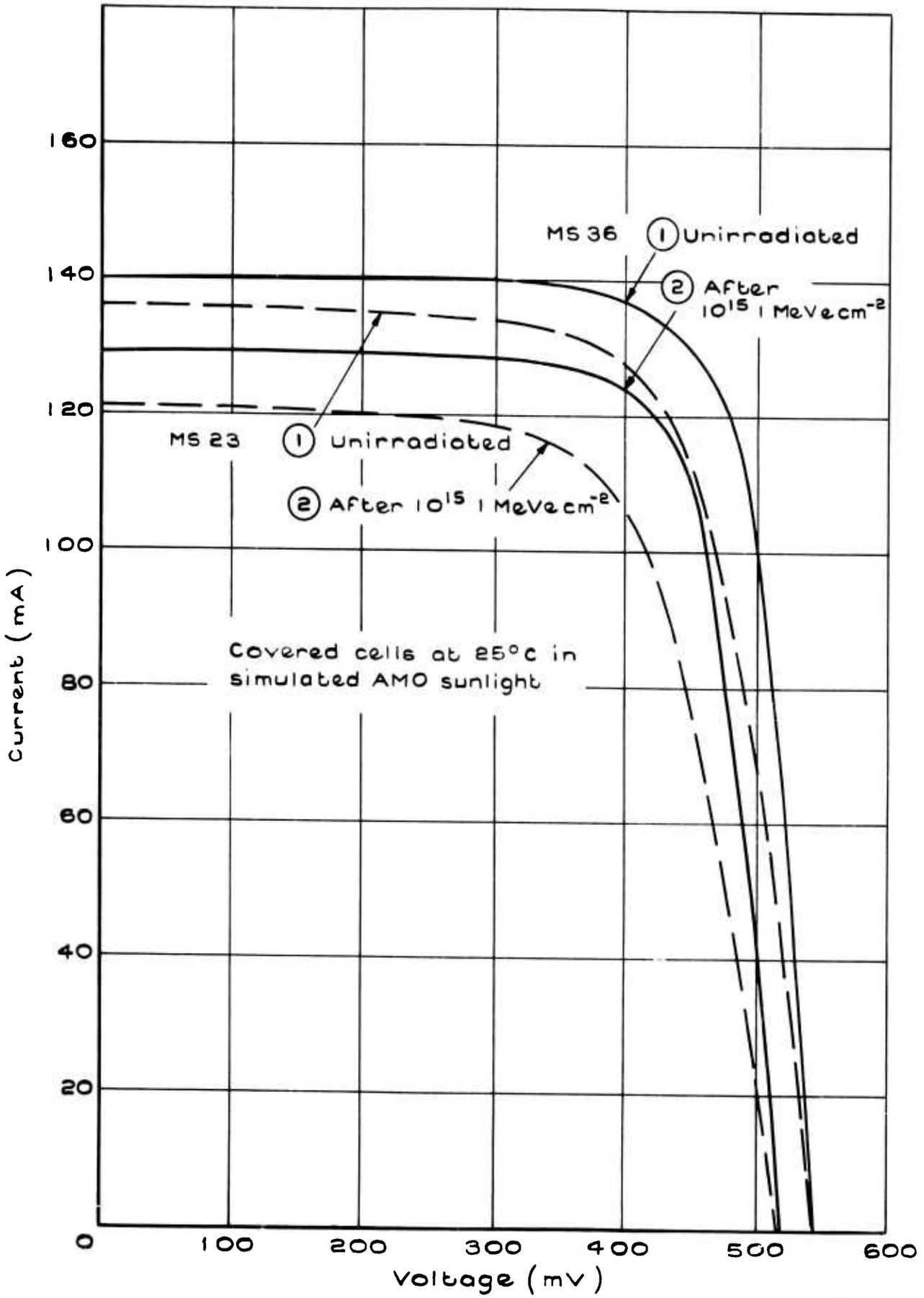

T.R.73105

Fig.19 Voltage-current characteristics of MS23 and MS36 cells

Fig. 20

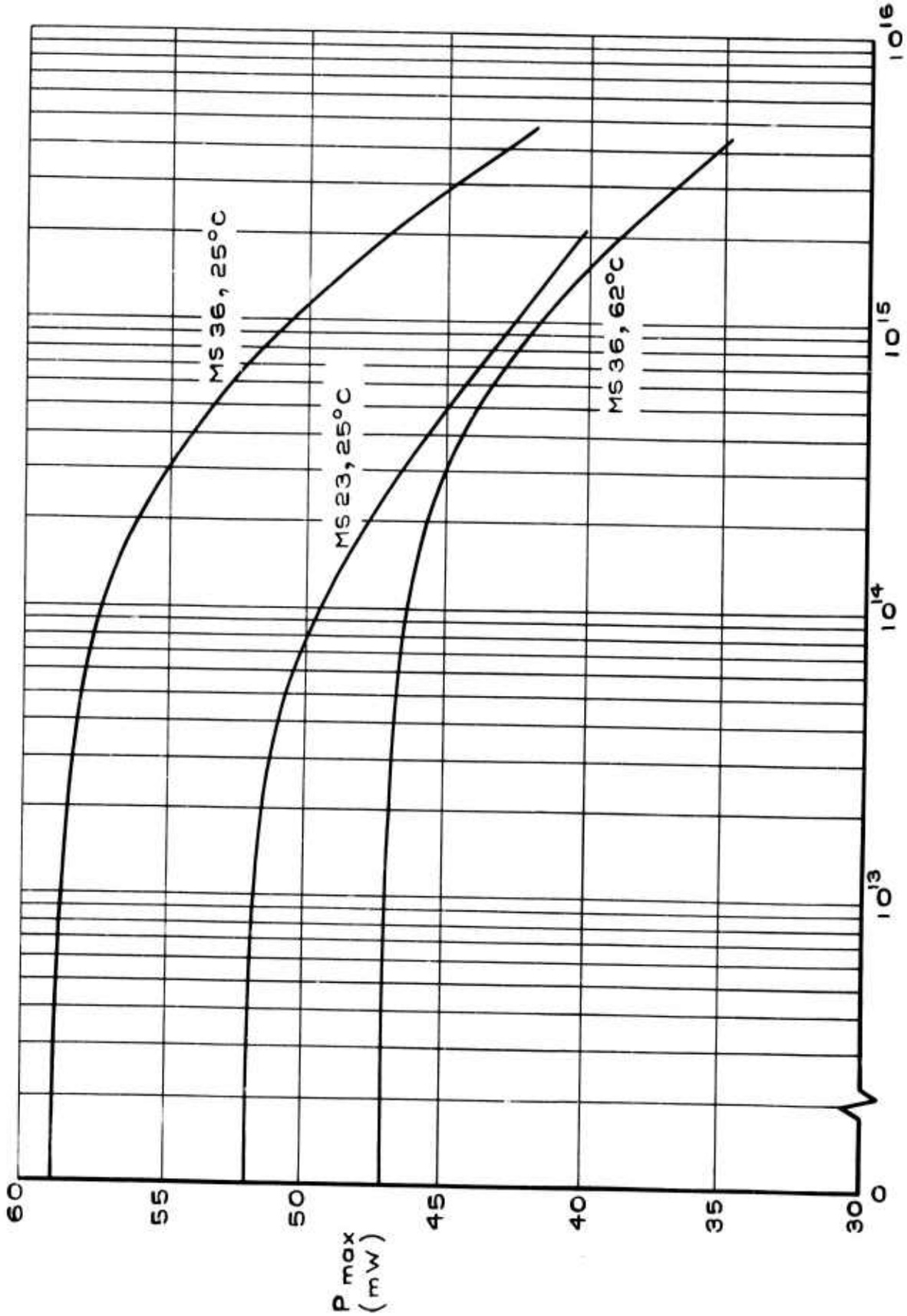

Fig. 20 Cell maximum power versus 1 MeV electron fluence

T.R.73105

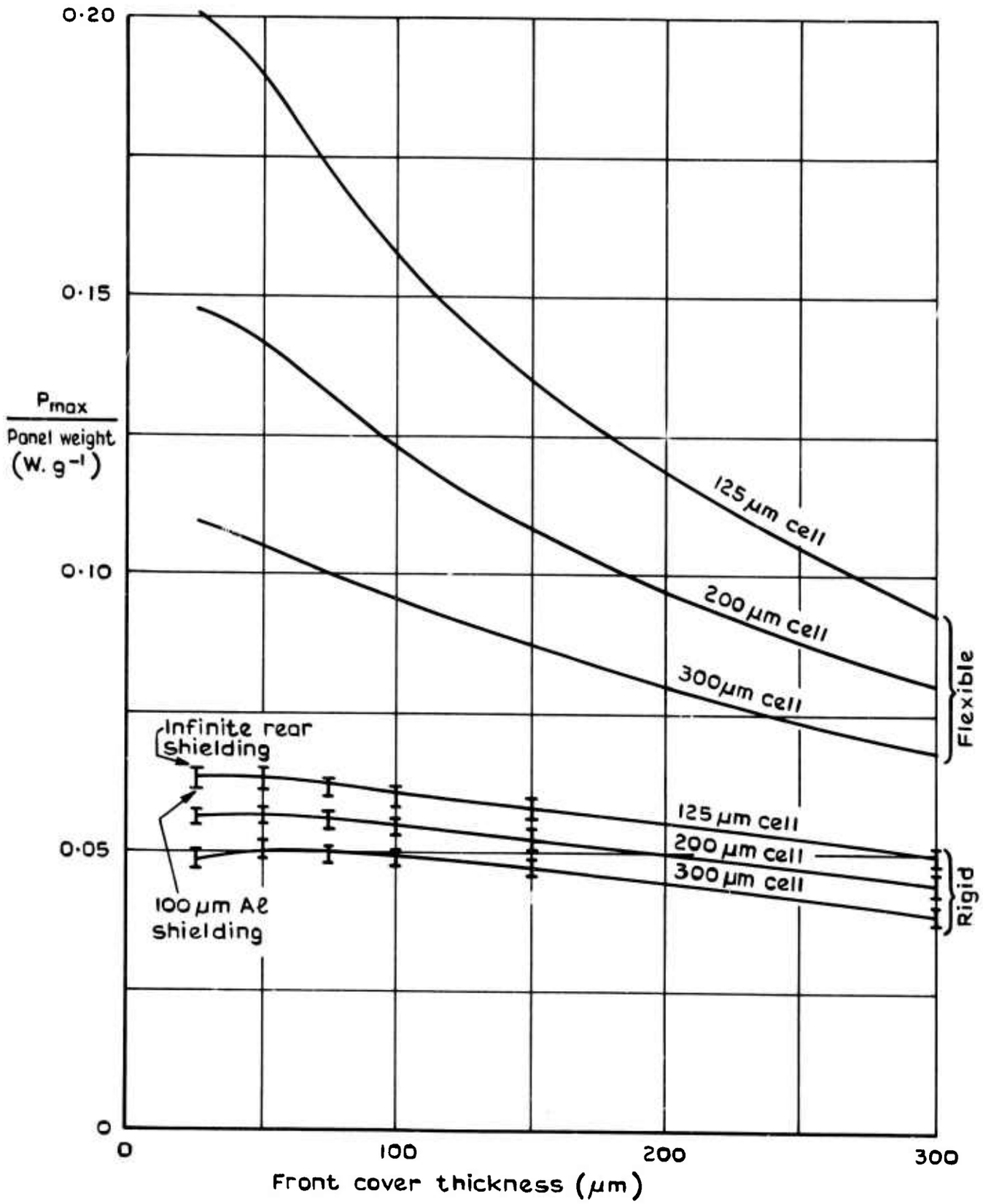

T.R.73105

Fig.21 Power to weight ratios